Wetting and Drying in Coastal Flows

Rodney J. Sobey
Department of Civil and Environmental Engineering,
Imperial College London,
London SW7 2AZ, UK
Phone: +44 (0)20 7594 5995, Fax: +44 (0)20 7594 5991
E-mail: r.j.sobey@imperial.ac.uk

Coastal Engineering, 56, 565-576, 2009

27 November 2008

Abstract

A complete description is presented of the physics of the wetting and drying or long wave runup of free surface coastal flows. A careful analysis of the front kinematics recognises the front as a material surface for which exact descriptions are provided. The limiting calculus at the front leads to a similarly exact description of the characteristic path of the wetting and drying front. The utility of this complete specification of the front kinematics is demonstrated in a method of lines algorithm. Visually perfect agreement is shown with two nonlinear analytical solutions.

Keywords Boundary friction, front kinematics, long waves, natural boundaries, numerical code, short waves, tides, tsunami runup, unsteady flow, wave runup, wetting and drying.

1 Introduction

Wetting and drying is a familiar feature of numerous coastal, estuarine and wetland flows. In natural bays and estuaries with a moderate to large tide range, the flow domain shrinks considerably from high to low tide stages. The impact on local navigation and on the local flow recirculation and contaminant transport are visually apparent. For storm tides and tsunamis, the runup of the wetting interface is perhaps the dominant issue. Often also, there is interest in the run-down of the drying interface in the potential impact on cooling water intakes and wastewater outfalls. In tidal wetlands, the physical and ecological interest often centres on the flow in the neighbourhood of the wetting and drying front.

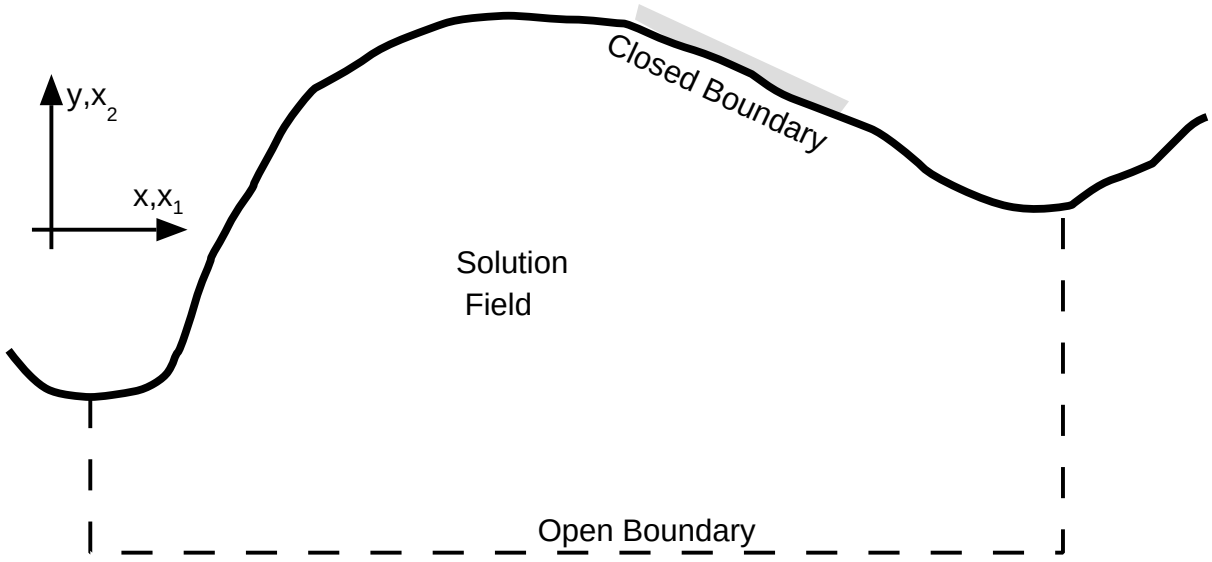

Figure 1: A two dimensional coastal basin.

In many numerical studies of coastal and estuarine flows, wetting and drying is assumed to be a peripheral process. And its representation is given little more than cosmetic attention. Often, this is an acceptable engineering approximation. But in a number of other situations, such as those highlighted above, the flow pattern in the neighbourhood of the wetting and drying interface is a specific concern. It is important then to get the physics correct. This is a lightly damped hyperbolic system, and any inaccuracy in the movement of the interface will be interpreted by the numerical code as forcing and rapidly propagated throughout the flow domain. Serious contamination of the entire domain prediction may result.

A closely associated issue is the discrete representation of natural boundaries. The accuracy of discrete approximations is mostly optimal on a uniform grid. A moving front will not correspond with a uniform grid, a reality that must be accommodated where fidelity at the wetting and drying interface is sought.

It is the purpose of this paper to describe the essential physics of the wetting and drying interface, to formulate a predictive model to capture that physics and to demonstrate the implementation of this predictive model in a sympathetic numerical code.

2 Conservation Equations

In two-dimensional coastal basins (the 2 dimensions referring to horizontal spatial direction x and y respectively; see Figure 1), the depth-integrated conservation equations are

$$\frac{\partial}{\partial t}\left(h+\eta\right)+\frac{\partial q_x}{\partial x}+\frac{\partial q_y}{\partial y}=0$$
$$\frac{\partial q_x}{\partial t}+\frac{\partial}{\partial x}\left(\frac{q_x^2}{h+\eta}\right)+\frac{\partial}{\partial y}\left(\frac{q_x q_y}{h+\eta}\right)-f_C q_y=-g\left(h+\eta\right)\frac{\partial \eta}{\partial x}+\mathbf{D}_x-\frac{\tau_{bx}}{\rho}+\mathbf{f}_x \qquad (1)$$
$$\frac{\partial q_y}{\partial t}+\frac{\partial}{\partial x}\left(\frac{q_x q_y}{h+\eta}\right)+\frac{\partial}{\partial y}\left(\frac{q_y^2}{h+\eta}\right)+f_C q_x=-g\left(h+\eta\right)\frac{\partial \eta}{\partial y}+\mathbf{D}_y-\frac{\tau_{by}}{\rho}+\mathbf{f}_y$$

These are depth-integrated mass and vector momentum equations in independent variables horizontal position x_α=(x,y) (α being 1 and 2) and time t. The dependent variables are local water surface elevation $\eta(x_\alpha,t)$ to a datum at the global MWL (mean water level), and the depth-integrated flow components $q_\alpha(x_\alpha,t)$. $h(x_\alpha)$ is the bathymetric field, with the bed at elevation z=$Z_b(x_\alpha)$=-$h(x_\alpha)$ to the MWL datum. f_C is the Coriolis coefficient, $\tau_{b\alpha}(x_\alpha,t)$ is the bed stress, and ρ is the mass density of water. The meteorological forcing is

$$\mathbf{f}_\alpha=-g\left(h+\eta\right)\frac{\partial}{\partial x_\alpha}\left(\frac{p_s}{\rho g}\right)+\frac{\tau_{s\alpha}}{\rho} \qquad (2)$$

which includes surface pressure $p_s(x_\alpha,t)$ and surface stress $\tau_{s\alpha}(x_\alpha,t)$ contributions.

$\mathbf{D}_\alpha$ in Equations 1b,c represents the dispersion terms in Boussinesq-style wave evolution equations that include the influence of non-gravitational contributions to the vertical pressure structure (e.g. Peregrine, 1967; Wei et al., 1995). For the purposes of the present discussion of runup or wetting and drying, it is unnecessary to be specific about the exact details of this complicated term.

The PDE system, Equations 1, is a nonlinear, initial boundary value problem. The listed equations are the so-called 2HD formulation, designating spatial variation in two horizontal spatial directions (x_α or x,y) and depth-integration in the vertical (z) direction. In the subsequent discussion, there is need also for a 1HD formulation (horizontal spatial variation in x only), where the conservation equations are

$$\begin{aligned}\frac{\partial}{\partial t}\left(h+\eta\right)+\frac{\partial q}{\partial x}&=0\\ \frac{\partial q}{\partial t}+\frac{\partial}{\partial x}\left(\frac{q^2}{h+\eta}\right)&=-g\left(h+\eta\right)\frac{\partial \eta}{\partial x}+\mathbf{D}-\frac{\tau_b}{\rho}+\mathbf{f}\end{aligned} \qquad (3)$$

3 Kinematics of the Wetting and Drying Front

The primary objective must be a viable predictive capability for the wetting and drying front, as encountered routinely in coastal waters. Routine predictive success (following Carrier and Greenspan, 1958) has been achieved under the very special conditions of a uniformly sloping beach, no short wave dispersion, no bottom friction and no meteorological forcing. In this context, a nonlinear transformation of the independent and dependent variables removes the need to consider the kinematics of the front. But these every special conditions do not correspond to the natural coastal environment, which imposes a much more general problem where the sea bed slope need not be uniform, and where short wave

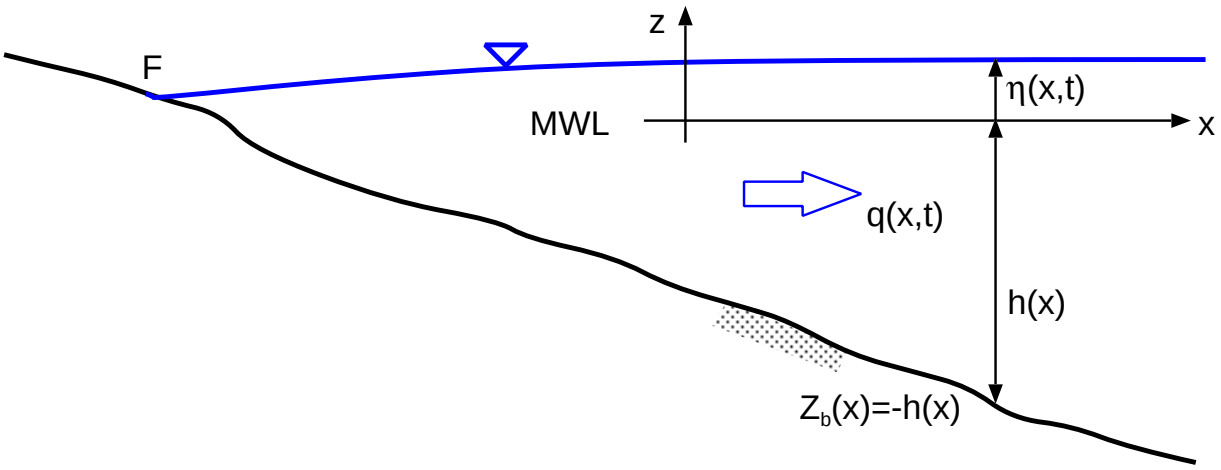

Figure 2: Definition Sketch in 1HD.

dispersion, bottom friction and meteorological forcing need not be zero. For the natural coastal environment, the expedient of the Carrier and Greenspan nonlinear transformation is not possible. The kinematics of the front must be directly addressed.

Consider initially a 1HD description of the wetting and drying front, Figure 2. At the front F,

(1) the local water surface elevation $\eta(x_F, t)$ and the local bed elevation $Z_b(x_F)$ coincide,

(2) the local water depth is zero,

$$h(x_F) + \eta(x_F, t) = \eta(x_F, t) - Z_b(x_F) = 0 \tag{4}$$

(3) the local depth-integrated flow per unit width is zero,

$$q(x_F, t) = 0 \tag{5}$$

(4) but the interface F moves at the potentially finite velocity

$$\frac{dx_F}{dt} = U(x_F, t) \tag{6}$$

The interface or front is recognised as a material surface where

$$\frac{D}{Dt}(\eta - Z_b) = 0 \quad \text{at } x_F \tag{7}$$

$$\text{and} \quad \frac{Dq}{Dt} = 0 \quad \text{at } x_F \tag{8}$$

Expanding the material derivatives, these become

$$\frac{\partial \eta}{\partial t} + U\frac{\partial \eta}{\partial x} = U\frac{\partial Z_b}{\partial x} \quad \text{at } x_F \tag{9}$$

$$\frac{\partial q}{\partial t} + U\frac{\partial q}{\partial x} = 0 \quad \text{at } x_F \tag{10}$$

which, together with Equation 6, describe the kinematics of the wetting and drying front in 1HD.

It remains to predict the speed of the front $U(x_F, t)$. Defining the depth-averaged fluid speed as

$$\overline{\overline{U}}(x,t) = \frac{q(x,t)}{h(x) + \eta(x,t)} \tag{11}$$

there is an intuitive expectation that $\overline{\overline{U}}(x,t)$ will evolve smoothly to $U(x_F, t)$ as x approaches x_F, i.e.

$$U(x_F, t) = \lim_{x \to x_F} \frac{q(x,t)}{h(x) + \eta(x,t)} \tag{12}$$

But the right hand side becomes $0/0$ and undefined at x_F. From l'Hôpital's rule however,

$$U(x_F, t) = \left. \frac{\partial q/\partial x}{\partial h/\partial x + \partial \eta/\partial x} \right|_{x=x_F} \tag{13}$$

In the unlikely event that the right hand side is also $0/0$, a further application of l'Hôpital's rule defines the front speed in terms of second spatial derivatives at the front.

The association of Equations 6, 11 and 13 with the characteristic paths at and in the neighbourhood of the front is instructive. Within the solution domain, the characteristic paths of the 1HD conservation Equations 3 are

$$\frac{dx}{dt} = \overline{\overline{U}} \pm \sqrt{g\,(h + \eta)} \tag{14}$$

At the front F, the shallow water phase speed becomes zero, and the Equation 14 characteristic paths coalesce to the single path Equation 6.

In a 2HD description, the interface or front moves at

$$\frac{d}{dt}\,(x_{F\alpha}) = U_\alpha(x_{F\alpha}, t) \tag{15}$$

where $x_{F\alpha}$ is the horizontal location at the boundary. The interface or front remains a material surface where

$$\frac{D}{Dt}\,(\eta - Z_b) = 0 \quad \text{at } x_{F\alpha} \tag{16}$$

$$\text{and} \quad \frac{Dq_\alpha}{Dt} = 0 \quad \text{at } x_{F\alpha} \tag{17}$$

Expanding the material derivatives, these become

$$\frac{\partial \eta}{\partial t} + U_\beta \frac{\partial \eta}{\partial x_\beta} = U_\beta \frac{\partial Z_b}{\partial x_\beta} \quad \text{at } x_{F\alpha} \tag{18}$$

$$\frac{\partial q_\alpha}{\partial t} + U_\beta \frac{\partial q_\alpha}{\partial x_\beta} = 0 \qquad \text{at } x_{F\alpha} \tag{19}$$

which, together with Equation 15, describe the kinematics of the wetting and drying front in 2HD. Here, α and β are 1 and 2.

Using l'Hôpital's rule as for 1HD,

$$U_\alpha(x_{F\alpha}, t) = \left(\frac{\partial q_x/\partial x}{\partial h/\partial x + \partial \eta/\partial x}, \frac{\partial q_y/\partial y}{\partial h/\partial y + \partial \eta/\partial y} \right) \Bigg|_{x=x_F, y=y_F} \tag{20}$$

These kinematic conditions, Equations 6, 9, 10 and 13 in 1HD and Equations 15, 18, 19 and 20 in 2HD, exactly and continuously describe the boundary conditions at the moving boundary of the flow domain. Used simultaneously with the mass and momentum conservations equations for the flow domain, the mathematical formulation for an appropriate predictive model is complete.

4 Wetting and Drying Approximations

Literature predictions for the wetting and drying front are numerous but rarely approach the potential fidelity implicit in the exact formulation above.

An immediate issue is the mathematical nature of the problem formulation, namely Eulerian or Lagrangian. The moving boundary suggests consideration of a Lagrangian formulation. This has been attempted in a 1HD analysis (Zelt, 1991), but is unfamiliar in practice and inconvenient in interpretation. It will not be pursued.

The most familiar and convenient algorithm adopts a fixed Eulerian grid in horizontal space, and the following discussion will assume this context.

Common computational algorithms (finite difference, finite element, ...) are discrete in space and discrete in time. The wetting and drying front is a moving boundary and discontinuous translations of the boundary each time step will drive spurious transients in the flow domain. Where these transients appear as high frequency oscillations, they may be immediately recognisable. But in a lightly damped hyperbolic problem, any local change, be it physical or even partially erroneous, is propagated as a disturbance. Error recognition is not transparent.

Fixed Grid. One approach to avoid these transients is to retain a fixed grid over the wetting and drying domain by never allowing any computational cell to completely dry. Measures include

(a) the Priessmann slot (Preissmann and Cunge, 1961). A deep but narrow slot in the bed always leaves a wet cell. The assigned geometry of the slot has a major influence on the predictions.

(b) wet-dry storage cells (Reid and Bodine, 1968; Leendertse and Gritton, 1971; Falconer and Owens, 1987; Oey, 2005). Cells are either completely inundated and "wet", or "dry" but retain a small minimum depth of water.

(c) porous or partly wet cells (King and Roig, 1988; Madsen et al., 1997; Bates and Hervouet, 1998). A diffusion-style assumption is introduced to smooth progressive inundation of cell.

These are pragmatic engineering approaches but, in each case, the kinematic boundary conditions, Equations 15, 18 and 19, are compromised.

Passive Nodes at Shoreline. Alternative efforts have accepted the moving boundary and sought a closer representation of the front physics.

One popular approach (e.g. Sielecki and Wurtele, 1970; Titov and Synolakis, 1995; Lynett et al., 2002, both in 1HD) to location of the moving front has been extrapolation from within the local flow domain. The instantaneous boundary is located at the intersection of the extrapolated water surface with the bed. This approach additionally ignores the kinematics of the moving front and perhaps also mass and momentum conservation in the immediate near-shore region.

Of the available literature approaches to wetting and drying, such extrapolation from within the local flow domain is a pragmatic practice that seems to yield reasonably plausible flow field predictions.

Active Nodes at Shoreline. Another popular approach (Lynch and Gray, 1980; Bellotti and Brocchini, 2001; Brocchini et al., 2002; Prasad and Svendsen, 2003) is based in part on the characteristic path Equation 6. Given Equation 6, it remains to predict the local velocity $U(x_F, t)$ of the front and to communicate the moving boundary prediction to the fixed Eulerian grid.

Introducing again the depth-averaged flow velocity $\overline{\overline{U}}$ (Equation 11), the 1HD depth-integrated conservations Equations 3 become

$$\begin{aligned} \frac{\partial}{\partial t}\left(h+\eta\right) + \frac{\partial}{\partial x}\left(\left(h+\eta\right)\overline{\overline{U}}\right) &= 0 \\ \left(h+\eta\right)\left(\frac{\partial \overline{\overline{U}}}{\partial t} + \overline{\overline{U}}\frac{\partial \overline{\overline{U}}}{\partial x}\right) &= -g\left(h+\eta\right)\frac{\partial \eta}{\partial x} + \mathbf{D} - \frac{\tau_b}{\rho} + \mathbf{f} \end{aligned} \tag{21}$$

For $(h+\eta) \neq 0$, Equation 21b may be divided through by $(h+\eta)$ to become

$$\frac{D\overline{\overline{U}}}{Dt} = -g\frac{\partial \eta}{\partial x} + \frac{\mathbf{D} - \tau_b/\rho + \mathbf{f}}{h+\eta} \tag{22}$$

But the transformation from Equation 21b to 22 is appropriate only for finite $(h+\eta)$. At the front, $(h+\eta) = 0$, and this is division by zero. In the derivation of the depth-integrated

conservation equations, the depth integration becomes trivial as the lower and upper limits of depth integration correspond.

Nevertheless, Lynch and Gray (1980), Brocchini et al. (2002) and Prasad and Svendsen (2003) interpret Equation 22 at the front as

$$\frac{dU_F}{dt} = -\,g\frac{\partial \eta}{\partial x}\bigg|_F \tag{23}$$

This is a flawed methodology.

Grid resolution near the shoreline becomes an issue where there is an active and moving node at the boundary. Grid spacings at the front evolve both in and out with the moving front, leading to potentially extreme distortions in the grid. Grid non-uniformity to this extent is generally associated with severely declining numerical precision. Accommodating measures have been re-meshing (Lynch and Gray, 1980) and coordinate and conservation equation transformations (Brocchini et al., 2002).

5 Natural Boundaries

The designation of natural boundaries is inevitably associated with a nonuniform local grid spacing. It is useful to recall what compromises may be involved, as they are potentially significant in the subsequent discussion.

Consider, for example the spatial derivative $\partial q/\partial x$ in Equation 3a or $\partial \eta/\partial x$ in Equation 3b, or generically $\partial f/\partial x$. On a locally non-uniform grid (see Figure 3 near F), the

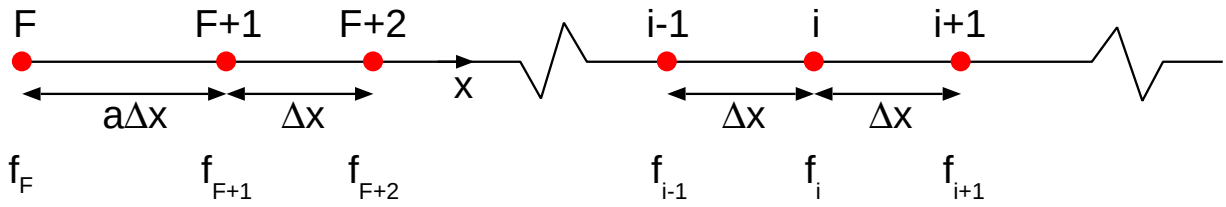

Figure 3: Locally non-uniform 1HD grid at Left Hand Boundary.

lowest order approximation at node F+1 (e.g. Ames, 1969, Section 1-9) that is centred (i.e. involves neighbouring nodes to both sides of node F+1) is

$$\frac{\partial f}{\partial x}\bigg|_{F+1} = \frac{-f_F + (1-a^2)f_{F+1} + a^2 f_{F+2}}{a(a+1)\Delta x} - \frac{\partial^3 f}{\partial x^3}\bigg|_{F+1}\frac{a\Delta x^2}{6} + \ldots \tag{24}$$

This approximation is established from Taylor series expansion about node F+1 for the neighbouring nodes F and F+2. The expansion is grouped in an optimal manner to cancel the lowest order truncation error, the Taylor series term involving $\partial^2 f/\partial x^2|_{F+1}$. The

truncation error is second order, $O(\Delta x^2)$, and does not require the grid to be uniform. For a uniform grid, a=1 and Equation 24 becomes a very familiar result.

Note that a local quadratic approximation for f,

$$f(x) = F_2 x^2 + F_1 x + F_0 \tag{25}$$

constrained to pass through f_F, f_{F+1} and f_{F+2} at x=-$a\Delta x$, 0 and Δx respectively has coefficients

$$F_2 = \frac{f_F - (1+a) f_{F+1} + a f_{F+2}}{a(1+a)\Delta x^2}, \quad F_1 = \frac{-f_F + (1-a^2) f_{F+1} + a^2 f_{F+2}}{a(1+a)\Delta x}, \quad F_0 = f_{F+1} \tag{26}$$

At x=0, $\partial f/\partial x|_{F+1}$=$F_1$, which is the same result as Equation 24. Local second order (quadratic) interpolation corresponds to second order precision, even for a non-uniform grid.

At a boundary node, such as F in Figure 3, a non-centred approximation is not available but a 3-point quadratic approximation over nodes F, F+1 and F+2 for $\partial f/\partial x$ at F is

$$\left.\frac{\partial f}{\partial x}\right|_F = \frac{-(1+2a) f_F + (1+a)^2 f_{F+1} - a^2 f_{F+2}}{a(1+a)\Delta x} + \left.\frac{\partial^3 f}{\partial x^3}\right|_F \frac{a(1+a)\Delta x^2}{6} + \ldots \tag{27}$$

This approximation, from local Taylor series expansion or local quadratic approximation, remains second order accurate.

The dispersion term **D** in Equations 3b may include gradients of dependent variables (η and/or q) higher than one. A 3-point centred approximation for a second derivative term at F+1 is

$$\left.\frac{\partial^2 f}{\partial x^2}\right|_{F+1} = \frac{f_F - (1+a) f_{F+1} + a f_{F+2}}{a(1+a)\Delta x^2} - \left.\frac{\partial^3 f}{\partial x^3}\right|_{F+1} \frac{(1-a)\Delta x}{3} - \left.\frac{\partial^4 f}{\partial x^4}\right|_{F+1} \frac{(1-a+a^2)\Delta x^2}{12} + \ldots \tag{28}$$

This result is second order accurate only where a=1, corresponding to a uniform grid. Generally for a non-uniform grid, $\partial^2 f/\partial x^2$ will require a 4-point (cubic) approximation for second order precision, $\partial^3 f/\partial x^3$ a 5-point (quartic) approximation for second order precision, ... The overall precision is dictated by the precision of the lowest order approximation, which will correspond with the highest order term. Where higher order dispersion terms are involved, there is a definite precision advantage is adopting a uniform grid wherever possible.

In 2HD, the details (Thacker, 1977, 1979) are conceptually identical though algebraically more complicated. But the conclusions are consistent. For example, a local bi-quadratic in x, y will provide second order precision for $\partial f/\partial x$ and $\partial f/\partial y$.

The finite element method is not immune to these issues. Discrete approximations to the same term to exactly the same order of approximation must be identical, regardless of the manner of local interpolation. Local interpolation in the finite difference method adopts Taylor series approximations. Local interpolation in the finite element method adopts shape functions. Both are local polynomial approximations (linear, quadratic, ... or bi-linear, bi-quadratic, ...). The finite element method does not dwell on local truncation errors, but the issues are identical.

6 Boundary Shear in Shallow Water

The expected balance of terms in the momentum Equation 3b in the neighbourhood of the wetting and drying front is instructive. Ignoring for the present the contributions from dispersion and meteorological forcing, the balance explicit in Equation 3b is

$$\text{Inertia} = \text{Gravity} - \text{Boundary Shear} \tag{29}$$

In all but very shallow water, this balance in long wave flows is dominated by the inertia and gravity contributions, with boundary shear having a rather less significant role.

The common quadratic model for boundary shear is

$$\text{Boundary Shear} = \frac{\tau_b}{\rho} = \frac{f}{8}\left|\overline{\overline{U}}\right|\overline{\overline{U}} \tag{30}$$

The Darcy-Weisbach friction factor f can be estimated from the Moody diagram, where f is approximately (Colebrook and White, 1937)

$$\frac{1}{f^{1/2}} = -2\log_{10}\left[\frac{k_s/D}{3.71} + \frac{2.51}{\mathbf{Re}f^{1/2}}\right] \text{ for } \mathbf{Re} >> 2000 \tag{31}$$

in which D is the pipe diameter and $\mathbf{Re}$ is the Reynolds Number. For high Reynolds Number open channel flow, the friction factor from Equation 31 becomes

$$f = \left[\log_{10}\left(\frac{k_s/\left(h+\eta\right)}{14.8}\right)^{-2}\right]^{-2} \tag{32}$$

In shallow water in the neighbourhood of the front, the roughness height k_s remains unchanged or perhaps increases and the local water depth $(h+\eta)$ rapidly decreases, so that the relative roughness $k_s/\left(h+\eta\right)$ rapidly increases. From Equation 32, the friction factor will increase significantly. The depth-averaged flow velocity $\overline{\overline{U}}$ is not expected to change significantly in the neighbourhood of the front, so that the boundary shear is expected to significantly increase on approach to the wetting and drying front.

In the Equation 29 momentum balance, boundary shear is expected to become increasingly important in the neighbourhood of the front.

7 The Predictive Challenge

Several observations follow from the above discussion:

(1) The exact kinematics of the wetting and drying front can be formulated (Section 3), but have yet to be completely implemented.

(2) Non-uniform grid spacings at natural boundaries need not compromise the numerical precision (Section 5).

(3) Bottom friction is expected to have a major influence on the translational speed of the wetting and drying front (Section 6)

(4) Only active boundary node algorithms have the potential to represent wetting and drying without compromise.

Accordingly, the present paper seeks to formulate an Eulerian methodology with the following constraints or characteristics:

(A) Generally fixed and spatially uniform grid, except in accommodating the natural boundary at the moving wetting and drying front.

A fixed uniform grid permits the use of the familiar conservation equations and avoids a mesh generation overhead. It also streamlines both the input of bathymetric and initial conditions and the output of solution evolution predictions in a manner most convenient for data display and interpretation.

(B) Smooth translation of the natural boundary, following Equations 6 and 9 in 1HD (or Equations 15 and 18 in 2HD).

The exact physics of the wetting and drying front should be implemented without compromise, leading to viable prediction of the evolution of the front.

(C) Bottom friction should be included in wetting and drying algorithm.

Bottom friction becomes increasingly influential at and near the wetting and drying front. Ignoring bottom friction would immediately identify a flawed algorithm.

(D) No compromise in numerical precision from a non-uniform grid at the natural boundary.

The non-uniform and evolving grid at the shoreline must be accommodated in a manner that achieves a numerical precision that is at least consistent with expected accuracy on a uniform grid.

Constraints A and B suggest an algorithm that is discrete and potentially non-uniform in space, but continuous in time. Only an algorithm that is continuous in time can successfully follow the moving front. On a fixed Eulerian grid, such an algorithm is the method of lines, as demonstrated elsewhere (Sobey, 2001) in a uniform grid 1HD context.

The continuously evolving front location must follow the exact kinematics (constraint B) with consistent numerical precision (constraint D), and must recognise dispersion, meteorological forcing and especially bottom friction (Equation 13 and constraint B) at and near the shoreline. This suggests that, in the neighbourhood of the shoreline, the full conservation equations must be imposed together with optimal spatial approximations (Section 5) that are consistent with the wider solution domain.

The following discussion will introduce and demonstrate such an algorithm in 1HD.

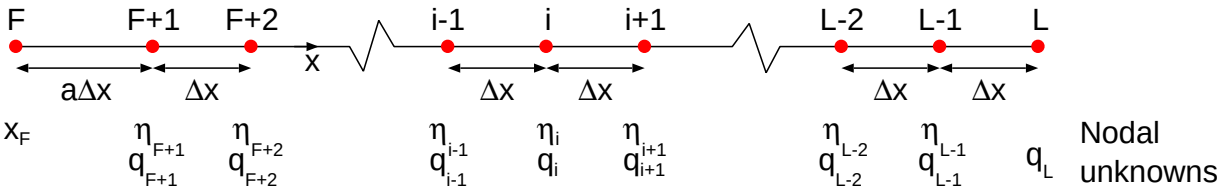

Figure 4: The 1HD discrete grid.

8 A 1HD Moving Boundary Algorithm

Consider a 1HD solution field with spatial node distribution as indicated in Figure 4. Internally, the spatial grid near node i is uniform with grid spacing Δx. At the front (e.g., in Figure 4, a left hand boundary), the immediate near-shoreline grid spacing (x_F to x_{F+1}) will generally not be Δx, though the adjacent internal spacings (e.g. x_{F+1} to x_{F+2}, and elsewhere throughout the domain) will be Δx.

The model unknowns are explicitly listed in Figure 4. At each internal node, they are η_i and q_i, i=(F+1),(F+2), ... i ... (L-2),(L-1) and L. At node F, the unknown is x_F. At node L, the unknown is q_L, where $\eta_L = \eta(x_L, t)$ is the given open boundary condition. Each of these listed unknowns are simultaneously predicted by first order ordinary differential equations, as described below.

Discrete Equations near Internal Node i. Near internal node i, the dependent variables are assumed to follow a locally quadratic variation, such that

$$\eta(x,t) = E_2(t)x^2 + E_1(t)x + E_0(t), \quad q(x,t) = Q_2(t)x^2 + Q_1(t)x + Q_0(t) \tag{33}$$

in the manner of Equation 25. From Section 5, the Equation 33 interpolation will achieve second order accuracy for gradient terms. The water depth and the combined dispersion, bottom friction and meteorological forcing are interpolated in similar manner, as

$$h(x) = H_2x^2 + H_1x + H_0, \quad \mathbf{D}(x,t) - \frac{\tau_0(x,t)}{\rho} + \mathbf{f}(x,t) = T_2(t)x^2 + T_1(t)x + T_0(t) \tag{34}$$

respectively. Substituting local interpolation Equations 33 and 34 into the 1HD conservation Equations 3 results in the simultaneous ordinary differential equation (ODE) pair at the node i

$$\begin{aligned} \left.\frac{d\eta}{dt}\right|_i &= -Q_1 \\ \left.\frac{dq}{dt}\right|_i &= -2\frac{Q_0Q_1}{H_0+E_0} + \frac{Q_0^2(H_1+E_1)}{(H_0+E_0)^2} - g(H_0+E_0)E_1 - T_0 \end{aligned} \tag{35}$$

to second order precision.

The physical contributions to the mass and momentum balances are clear in Equations 35. In Equation 35a, the left hand side is storage of mass and the right hand side advection of mass. In Equation 35b, the left hand side is storage of momentum. On the right hand side, the first and second terms are advection of momentum, the third term is gravity and the final term is the combined contribution from dispersion, bottom friction and meteorological forcing.

The local quadratic coefficients, generically F_0, F_1 and F_2 in Equations 33 and 34, are determined from the nodal values of $f(x)$, respectively $f_{i-1}(t)$, $f_i(t)$ and $f_{i+1}(t)$ at $x_i - \Delta x$, x_i and $x_i - \Delta x$. Accordingly,

$$F_0 = f_i, \quad F_1 = \frac{f_{i+1} - f_{i-1}}{2\Delta x}, \quad F_2 = \frac{f_{i+1} - 2f_i + f_{i-1}}{2(\Delta x)^2} \tag{36}$$

At each of the internal nodes i, there are two unknowns (η_i,q_i) and two equations (Equations 35).

Discrete Equation at Open Boundary Node L. At open boundary node L, η_L is a given boundary condition. q_L is predicted by the local momentum Equation 35b, except that the quadratic coefficients must be evaluated over a non-centred but uniformly-spaced set of local nodes at (L-2), (L-1) and L.

The nodal values are generically f_{L-2}, f_{L+1} and f_L at x_{L-2}, x_{L-1} and x_L respectively. Each of the f_{L-2}, f_{L+1} and f_L is locally known, either as the instantaneous value of the nodal unknown or as a given boundary condition. The local quadratic coefficients are

$$\begin{aligned} F_0 = f_L, \quad F_1 &= \frac{f_{L-2} - 4f_{L-1} + 3f_L}{2\Delta x} \\ F_2 &= \frac{f_{L-2} - 2f_{L-1} + f_L}{2\Delta x^2} \end{aligned} \tag{37}$$

Discrete Equations at Near-Boundary Node F+1. At adjacent boundary node F+1 (Figure 4), the local discrete equations remain Equations 35, except that the quadratic coefficients must now be evaluated over a non-uniform local node distribution.

The nodal values are generically f_F, f_{F+1} and f_{F+2} at x_F, x_{F+1} and x_{F+2} respectively. From Section 3, the instantaneous conditions at x_F are

$$\eta_F(t) = Z_b(x_F, t), \quad q_F(t) = 0, \quad h_F(t) = -Z_b(x_F, t) \tag{38}$$

so that f_F is defined. The local quadratic coefficients are

$$\begin{aligned} F_0 = f_{F+1}, \quad F_1 &= \frac{-f_F + (1-a^2)f_{F+1} + a^2 f_{F+2}}{a(1+a)\Delta x} \\ F_2 &= \frac{f_F - (1+a)f_{F+1} + a f_{F+2}}{a(1+a)\Delta x^2} \end{aligned} \tag{39}$$

where $a = (x_{F+1} - x_F)/\Delta x$. Second order accuracy is retained (Section 5) for gradient approximations for E_1, Q_1 and H_1 in Equations 35 at node F+1. At near-boundary nodes F+1, there are two unknowns (η_{F+1},q_{F+1}) and two equations (35).

Discrete Equation at Moving Boundary Node F. At moving boundary node F, η_F and q_F are known (see Section 3) but the position $x_F(t)$ of the front remains as an unknown. The closure equation is provided by the front kinematics, Equation 6,

$$\frac{dx_F}{dt} = U_F \qquad ([6])$$

in which U_F is provides by Equation 13. With consistent quadratic interpolation for the spatial gradients at F in Equation 13, second-order accuracy is maintained.

Numerical Solution Issues. The adopted Δx spatial numerical grid size much be sufficient to resolve the spatial variations of the initial conditions and the predicted response. Similarly, the time resolution of the given boundary conditions must be sufficient to resolve the variation in this time history.

The dimensional differences between Equations 6 [length/time], 35a [length/time] and 35b [(length/time)^2] and the associated magnitude differences is a recurring numerical issues in numerical hydrodynamics. It is adequately accommodated by introducing appropriate length and time scales, and completing the numerical solution in non-dimensional variables.

Time resolution of the numerically predicted evolution within the solution domain is not an issue. The local Equations 6 and 35 are integrated numerically by an error correcting, adaptive step size Runge-Kutta code (`ode45` in matlab). The time integration is essentially numerically exact.

In applications where the horizontal translation of the wetting and drying front is very much larger than Δx, spatial resolution at the front will become an issue. Predicted spatial gradients at F are crucially important (Equation 13) to the numerical accuracy at the front. While Equation 27 shows that the truncation error at the front is generically second order in Δx, it is strictly second order in $a\Delta x$. The expected precision will vary with a, and decline as a increases. In the Section 7 preferred context of a fixed Eulerian grid, the addition and removal of nodes immediately adjacent to the front at F is anticipated. This issue is not considered in the present study.

9 Algorithm Confirmation

An especially valuable analytical solution is provided by Carrier and Greenspan (1958). The context is a special case of the full 1HD problem, Equations 3, where the terms $\mathbf{D} - \tau_b/\rho + \mathbf{f}$ (diffusion + bed friction + atmospheric forcing) are identically zero and the topography is a uniformly sloping beach at slope α (See Figure 5). The nonlinear advective acceleration and gravity terms are retained in the momentum equation, so that this is a rare nonlinear analytical solution.

In the dimensional problem suggested by Figure 5, the independent variables are x and t, and the dependent variables are $\eta(x,t)$ and $q(x,t)$. The Carrier and Greenspan (1958) solution is presented as the potential $\varphi(\sigma,\lambda)$ in dimensionless independent variables $\sigma =$

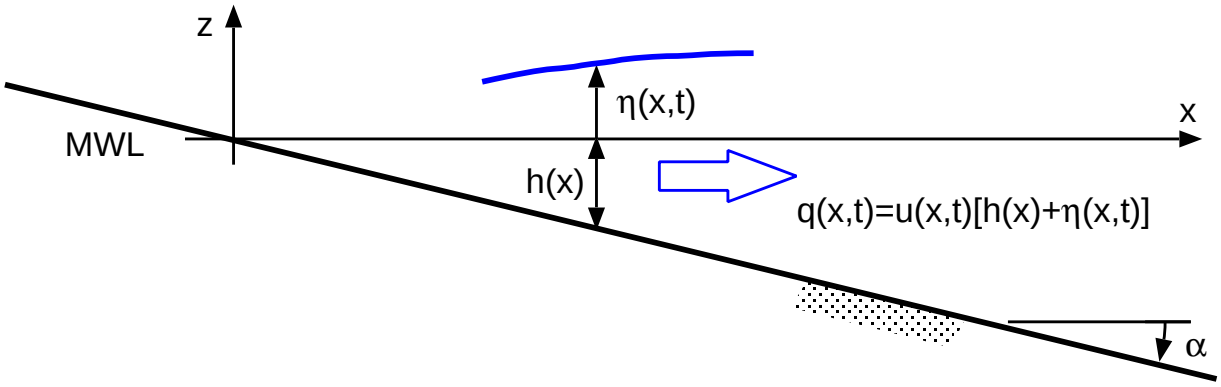

Figure 5: Definition Sketch for Carrier & Greenspan (1958) Analytical Solution in 1HD.

$\sigma(x,\eta)$ and $\lambda = \lambda(t,\overline{\overline{U}})$, where $\overline{\overline{U}} = q/(h+\eta)$ (Equation 11). Extraction of the dimensional dependent variables $\eta(x,t)$ and $q(x,t)$ at specified dimensional independent variables x and t requires the numerical solution of an inverse problem, described in Appendix A.

Test Case 1. The first test case adapts the Carrier and Greenspan (1958) context to tidal wetting and drying. The dimensionless amplitude A_1 is 0.4, the dimensional incident wave frequency is $2\pi/T_1$ where T_1 is 12.5 hours. The numerical solution domain extends to x_L=10000 m and the bed slope α is 0.001. The adopted uniform grid spacing Δx is 500 m. The initial conditions $\eta(x,0)$ and $q(x,0)$ and the boundary condition $\eta(x_L,t)$ are taken directly from the Carrier and Greenspan (1958) solution; they are shown in Figure 6. Note especially that $\eta(x,0)$ is not zero and varies with x. Also $\eta(x_L,t)$ is not exactly sinusoidal, though this is not apparent at the scale of Figure 6. Both are a consequence of the nonlinearity of the analytical solution.

The most sensitive aspects of the numerical solution are at the open boundary at x_L and at the moving front at $x_F(t)$. At both locations, the discrete equations involve non-centred quadratic approximations.

At the open boundary, $\eta(x_L,t)$ is provided as a boundary condition but $q(x_L,t)$ is predicted by the ODE Equation 35b with $Q_1 = \partial q_L/\partial x$ and $E_1 = \partial \eta_L/\partial x$ at x_L estimated from a quadratic approximation over the nodes x_{L-2}, x_{L-1} and x_L. The numerically and analytically predicted $q(x_L,t)$ traces are shown in Figure 7. Agreement is visually perfect.

At the wetting and drying front, the speed of the front $U(x_F,t)$ is predicted by Equation 13 and the position of the front $x_F(t)$ by the ODE Equation 6. The spatial gradients in Equation 13, $\partial q_F/\partial x$ and $\partial \eta_F/\partial x$, at x_F are estimated from a quadratic approximation over the nodes x_F, x_{F+1} and x_{F+2}, which is a non-centred approximation on a non-uniform grid (Equation 27). While this approximation is theoretically second order in Δx, it is specifically second order in $a\Delta x$. The dimensionless factor a remains of order 1, but will vary with time. Given $x_F(t)$, $\eta(x_F,t)$ is defined exactly by the bathymetry (Equation 9). $q_F(x_F,t)$ remains identically zero (Equation 10).

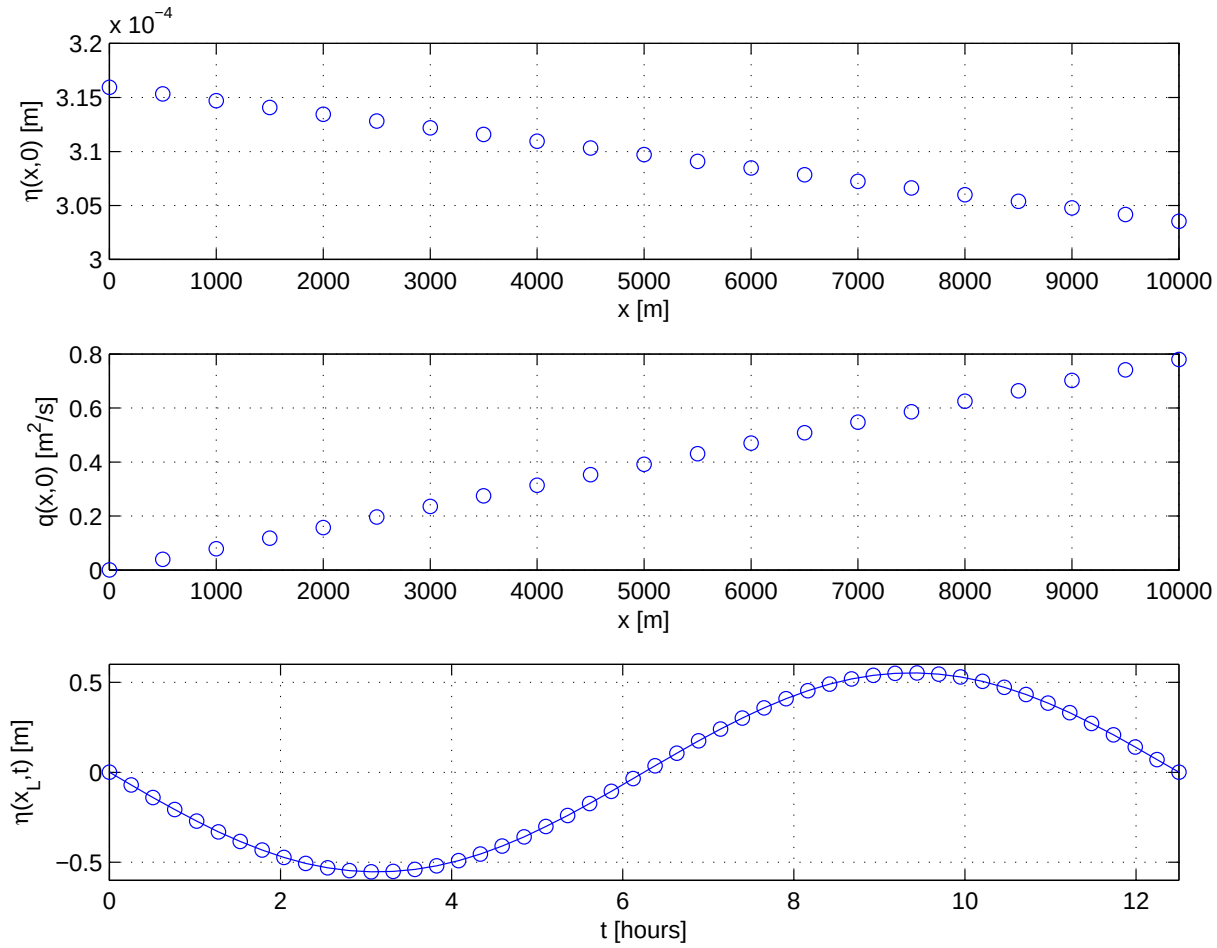

Figure 6: Test Case 1: Initial and Boundary Conditions.

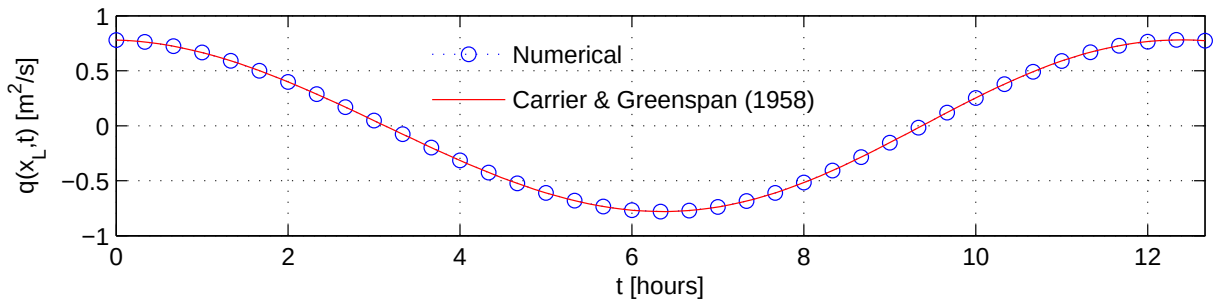

Figure 7: Test Case 1. Open Boundary $q(x_L, t)$ Prediction.

The numerically and analytically predicted $x_F(t)$ and $U(x_F, t)$ traces are shown in Figure 8. Agreement is again visually perfect.

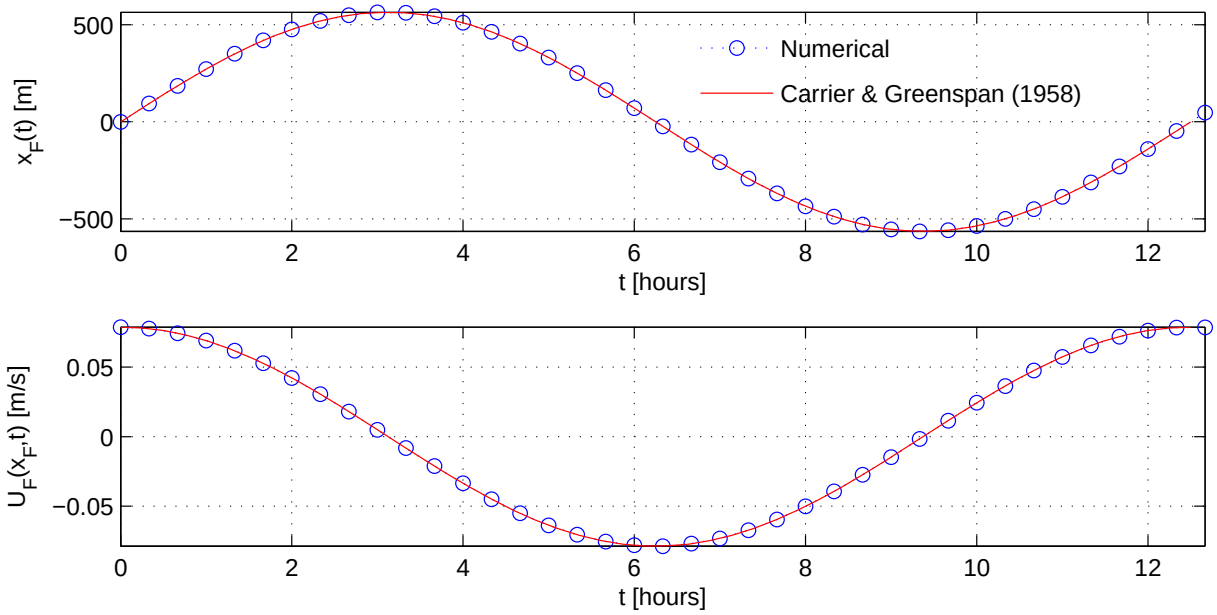

Figure 8: Test Case 1. $x_F(t)$ and $U(x_F, t)$ Predictions at Wetting and Drying Front.

It is appropriate to observe that Figures 7 to 8 are a very demanding test of both the problem formulation and the numerical code. There is no friction in this problem, so that this is an undamped hyperbolic wave system. Any error in either the problem formulation or the numerical code will be rapidly propagated as a disturbance throughout the flow domain at speeds of order $\sqrt{g\,(h(x)+\eta(x,t))}$. They will appear as oscillations in the flow predictions. None are observed.

Test Case 2. The second test case addresses tsunami runup, a context that involves both transient hydrodynamics and much shorter space and time scales in the response pattern. Once again, the test case is based on an analytical solution to the full 1HD problem, where the terms $\mathbf{D} - \tau_b/\rho + \mathbf{f}$ are identically zero and the topography is a uniformly sloping beach (See Figure 5). The solution adopted follows Tinti and Tonini (2005), as outlined also in Appendix A. The bed slope α is 0.1, the solution domain extends to x_L=3000 m, and Δx is 5 m. The adopted c_k coefficients are $[-1, 6, -2, -3]$.

The initial condition $\eta(x, 0)$ ($q(x, 0) = 0$) and the boundary condition $\eta(x_L, t)$ are taken directly from the Tinti and Tonini (2005) solution; they are shown in Figure 9. The very much smaller Δx spatial numerical grid size is necessary to resolve the more rapid spatial variations of the initial conditions and the predicted response.

At the open boundary, the numerically and analytically predicted $q(x_L, t)$ traces are shown in Figure 10. Agreement is again visually perfect.

At the wetting and drying front, the numerically and analytically predicted $x_F(t)$ and $U(x_F, t)$ traces are shown in Figure 11. Agreement is again visually perfect.

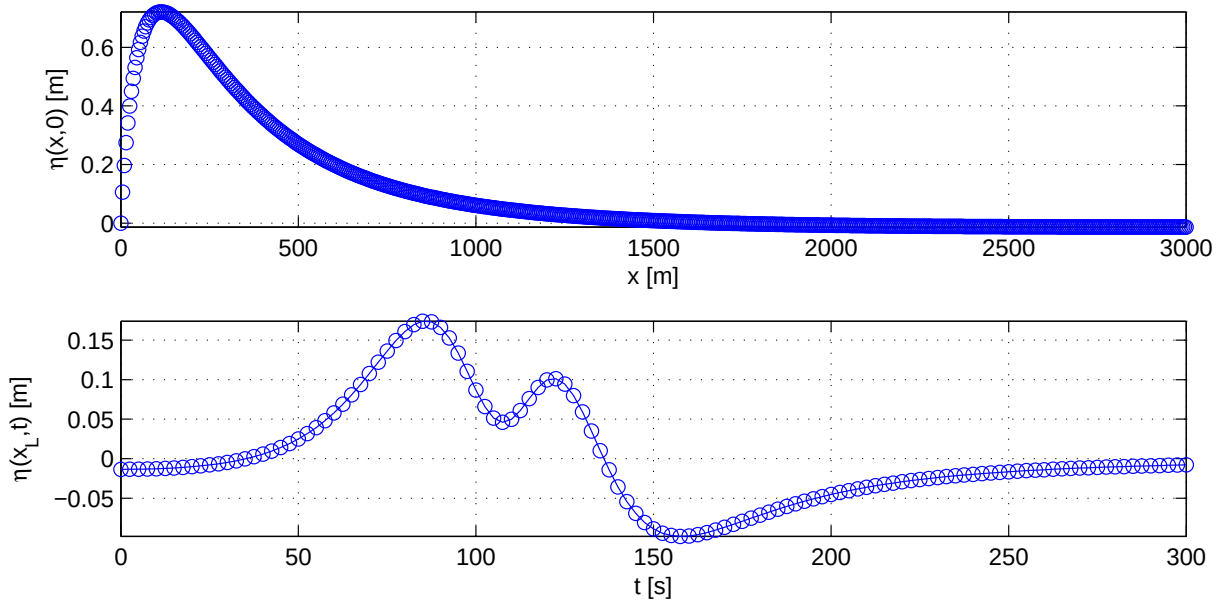

Figure 9: Test Case 2: Initial and Boundary Conditions.

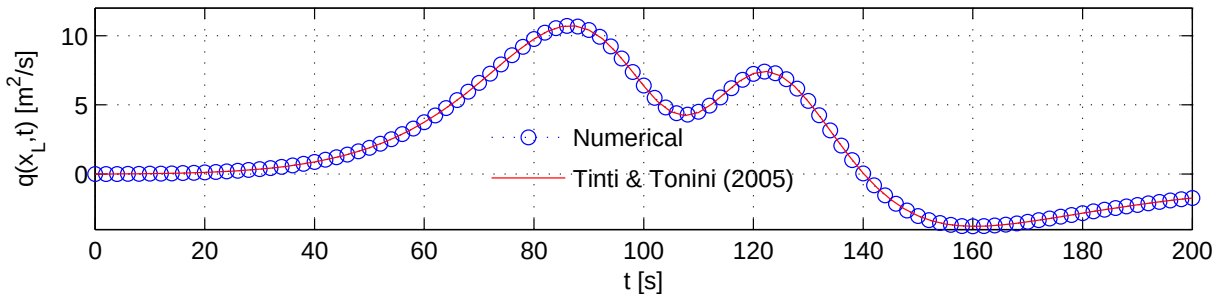

Figure 10: Test Case 2. Open Boundary $q(x_L, t)$ Prediction.

Unlike the tidal Test Case 1, there is significant spatial activity over the domain in this problem. The numerically and analytically predicted $\eta(x;t)$ profiles are shown in Figure 12. Plotting of the numerically predicted nodes has been considerably thinned away from the front, so as not to completely obscure the analytical solution. Agreement is again visually perfect.

Test Case 3. The final test case has no analytical solution but is a very basic tidal wetting and drying application. This problem retains the Test Case 1 bathymetry, but the friction coefficient f is not zero but 0.02 throughout. The initial conditions are quiescence,

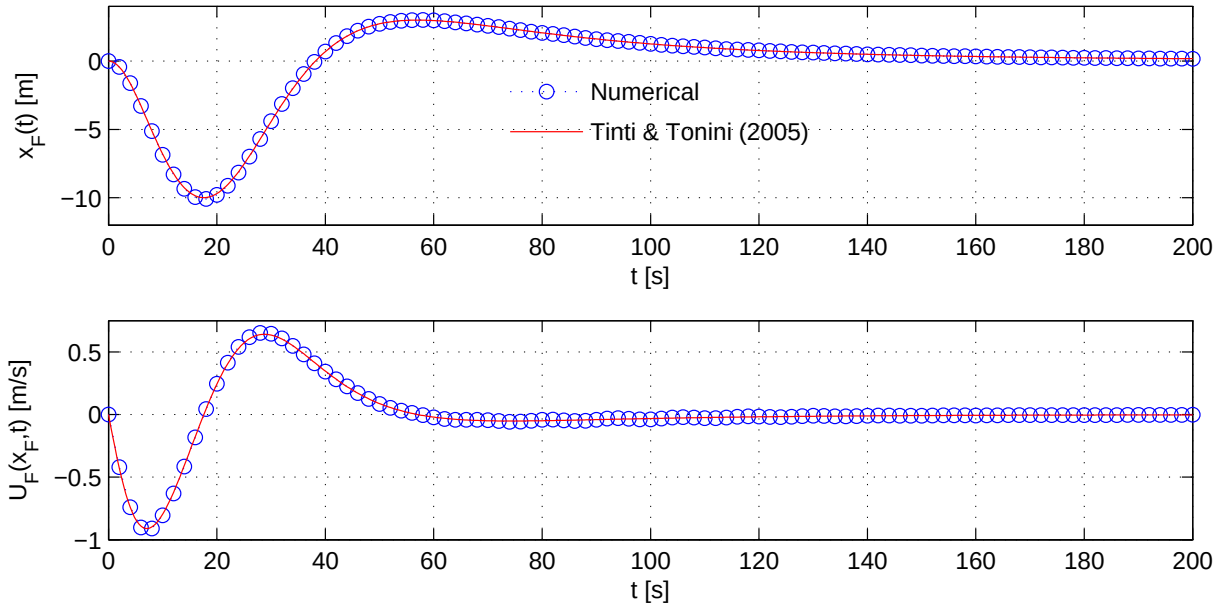

Figure 11: Test Case 2. $x_F(t)$ and $U(x_F, t)$ Predictions at Wetting and Drying Front.

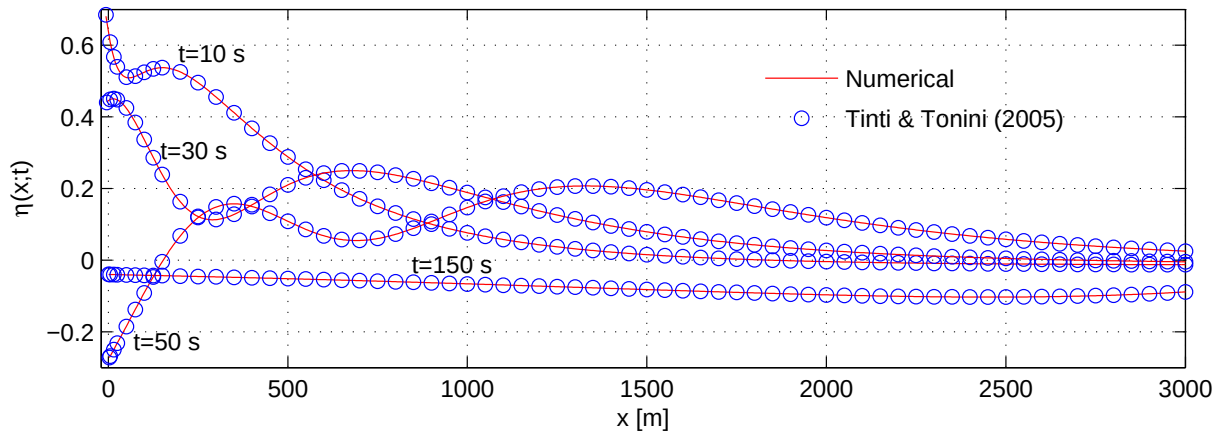

Figure 12: Test Case 2. Longitudinal Profile $\eta(x; t)$ Predictions at Selected Times.

$\eta(x, 0) = q(x, 0) = 0$, and the offshore boundary condition is the sinusoidal tide

$$\eta(x_L, t) = a_L \sin(\omega t) \tag{40}$$

where $a_L = 0.6$ m is the tidal amplitude and $\omega = 2\pi/12.5$ hours is the tidal frequency.

There is an immediate difficulty at the offshore boundary. There is a sudden change in $\partial\eta/\partial t$ at t=0, forcing a consequent sudden change in $\partial q/\partial x$ for local mass conservation

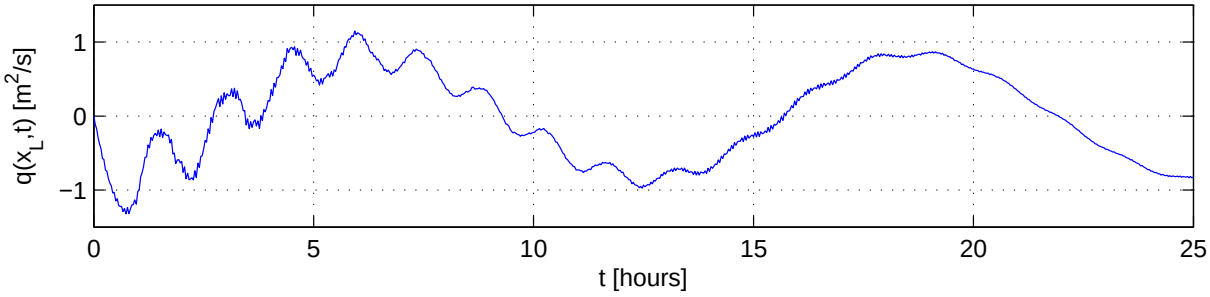

Figure 13: Test Case 3. Open Boundary $q(x_L, t)$ Prediction.

(Equation 3a). This sudden disturbance initiates a transient disturbance at the normal modes of the basin (Sobey, 2002). The eigenmodes for this computational domain (Lamb, 1932, pages 275-6) are

$$\eta(x,t) = a_n \frac{J_0(2\kappa_n^{1/2} x^{1/2})}{J_0(2\kappa_n^{1/2} x_L^{1/2})} \cos(\omega_n t + \phi_n) \tag{41}$$

where a_n is the amplitude, ω_n the frequency and ϕ_n the phase of the nth mode. $J_0()$ is the Bessel function of the first kind of order zero. $\kappa_n = \omega_n^2 x_L / g h_L$, in which $h_L = h(x_L)$, and the κ_n are defined by the zeros $\mathcal{Z}_n$ of the Bessel function $J_0(2\kappa_n^{1/2} x_L^{1/2})$. Accordingly, the eigenfrequencies are

$$\omega_n = \mathcal{Z}_n \frac{(g h_L)^{1/2}}{2 x_L} \tag{42}$$

The $\mathcal{Z}_n$ are 2.40, 5.52, 8.65, ... for n = 1,2,3, ... (Abramowitz and Stegun, 1964, Table 9.5) to three significant figures. The corresponding eigenmode periods are 87.9 minutes, 38.3 minutes, 24.4 minutes, ...

At the open boundary, the numerically predicted $q(x_L, t)$ trace is shown in Figure 13. The immediate excitation of the fundamental normal mode at a period of 87.9 minutes is clear, as is the slow frictional decay of this mode in the manner anticipated (Sobey, 2002). Initial transients of this nature are a routine feature (Bode and Sobey, 1984) of numerical modelling of the long wave equations. At the wetting and drying front, the numerically and analytically predicted $x_F(t)$ and $U(x_F, t)$ traces are shown in Figure 14. The initial transients and their slow friction decay once again dominate the immediate response pattern. There is evidence in the much more sensitive $U(x_F, t)$ trace also of the n=2 and perhaps n=3 modes. After two tidal cycles, the predicted patterns in both Figures 13 and 14 are evolving to the expected sinusoidal tide response. This is the routine "settling down time" of numerical long wave modelling.

A minor but physically significant issue is evident in the small scale of Figure 13. A high frequency noise persists through 20 hours. This is the notorious "$2\Delta x$" oscillations that are generated by spatial response patterns that are too short to be resolved by the adopted Δx resolution. In Figure 13, the "$2\Delta x$" oscillations are forced by the initial transient response

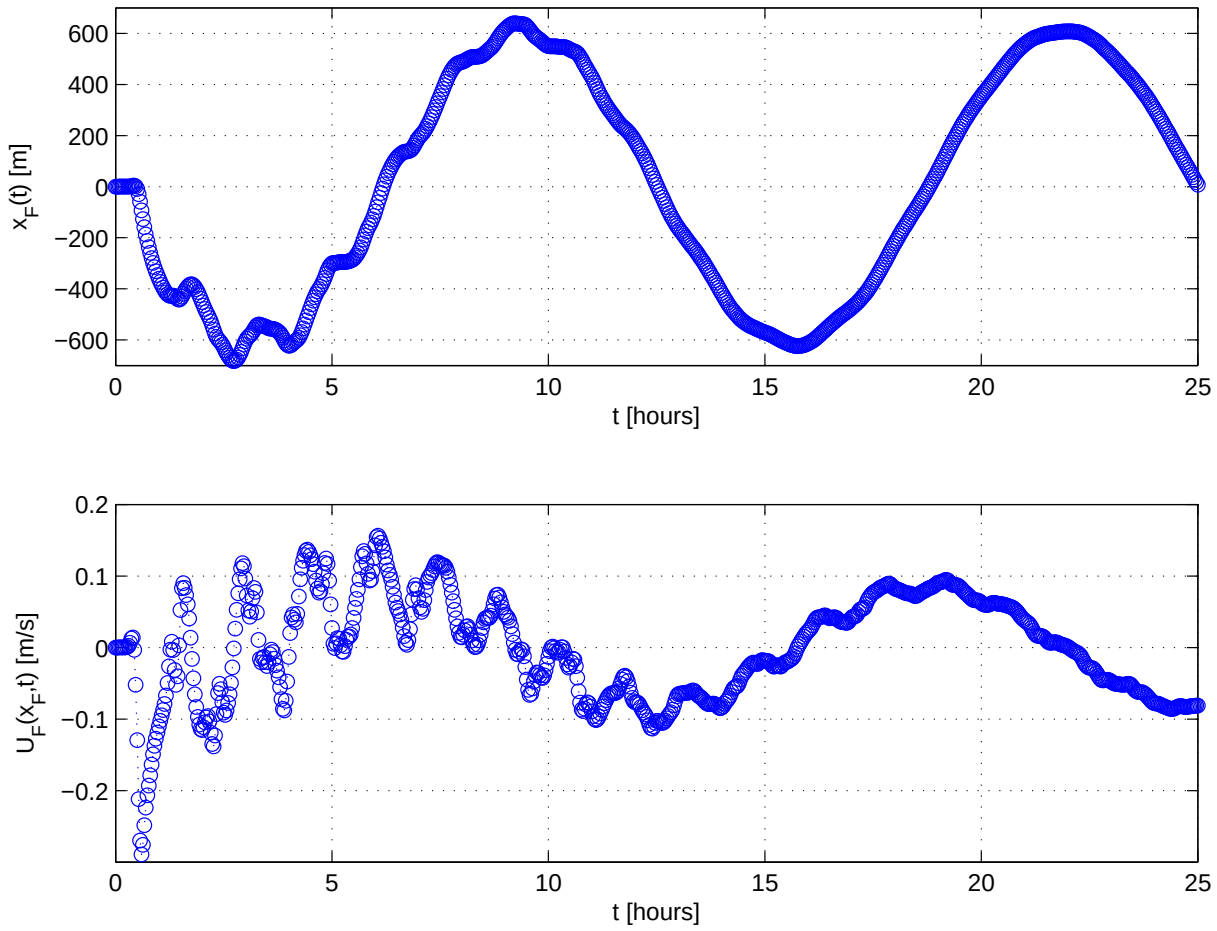

Figure 14: Test Case 3. $x_F(t)$ and $U(x_F, t)$ Predictions at Wetting and Drying Front.

at periods 87.9 minutes, 38.3 minutes, 24.4 minutes, ... that is very much shorter than the 12.5 hour period of the tidal forcing. The adopted spatial resolution would need to be very much smaller than 500 m to faithfully resolve these initial transients. As they have no relevance to the forced response and as the transients decay with time to friction, the adopted spatial resolution is routinely tuned to the forced response.

10 Further Application

The primary purpose of this paper has been to introduce an exact description of the front kinematics (Section 3). A secondary objective (Sections 5,7-9) has been to demonstrate the wide application of this exact description of the front kinematics to coastal flows through three selected Test Cases. These demonstrations focussed on non-breaking flows for very long waves (tides; Test Cases 1 and 3) and for somewhat shorter waves (tsunamis; Test Case 2). The numerical algorithm adopted for these Test Cases (Section 8) has no specific

capability to represent breaking waves within the solution domain.

The exact description of the front kinematics, as developed in Section 3, is dependent only on the kinematics in the immediate neighbourhood of the wetting and drying front, while the neighbouring flow remains gradually varied. There is no dependence on whether the neighbouring incident flow is an astronomical tide, a storm tide, a tsunami, a short wave, or a swash zone flow. The nature of the neighbouring incident flow will influence the field equations, which may or may not include breaking, dispersion and meteorological forcing. And the nature of this flow will impact the front boundary condition through the evolution of the spatial gradients of q and η at the moving front. But the exact kinematics at the front will remain those outlined in Section 3. Accordingly, the boundary condition at the wetting and drying front is unchanged across this spectrum of coastal problems, unless the immediately neighbouring flow is rapidly-varied.

Of course, the choice of a suitable numerical algorithm for the field solution will depend on the nature of the field equations, specifically whether or not they include

(a) dispersion,

(b) meteorological forcing, and/or

(c) wave breaking

Test Cases 1 through 3 include neither dispersion, nor meteorological forcing, nor breaking. Dispersion and meteorological forcing are expected to be accommodated without difficulty by the Section 8 algorithm. Wave breaking will likely require a rather different numerical algorithm, that will accommodate localised momentum sinks and rapidly-varied flow segments.

11 Conclusions

The wetting and drying front is described in 1HD as a material surface where the material derivative of both the water depth $(\eta - Z_b)$ and the depth-integrated flow q remain zero (Equations 9 and 10). At the front also, the positive and negative characteristic paths coalesce into the single characteristic path, Equation 6. An exact prediction for the speed $U(x_F, t)$ of the front is established from the limiting calculus of the front (Equation 13). These exact results are extended to 2HD in Equations 15 through 20.

The exact front kinematics are demonstrated in 1HD in a method of lines algorithm, based on Equations 35 augmented by Equation 13, in which the position $x_F(t)$ varies smoothly with time. Visually exact agreement is achieved with nonlinear analytical solutions for tidal wetting and drying (Test Case 1) and for tsunami runup (Test Case 2).

These are a very demanding tests of both the problem formulation and the numerical code. There is no friction in the analytical solutions. This is an undamped hyperbolic wave system. Any error in either the problem formulation or the numerical code will be rapidly propagated as a disturbance throughout the flow domain at speeds of order the

shallow water phase speed. They will appear as oscillations in the flow predictions. None are observed.

The final evaluation (Test Case 3) explore a typical numerical modelling application, the transition from quiescent initial conditions to a forced tide response. Boundary friction is not excluded from this problem. The startup is dominated by the familiar initial transients at basin normal modes. These decay slowly to friction, and the response evolves to the expected sinusoidal tidal response at the wetting and drying front.

A Implementation of Carrier & Greenspan (1958) Solution

The context of the Carrier and Greenspan (1958) analytical solution is the 1HD conservation Equations 3 with the terms $\mathbf{D} - \tau_b/\rho + \mathbf{f}$ identically zero and a topography that is a uniformly sloping beach at slope α (See Figure 5).

The solution transforms (Stoker, 1948) the independent variables x and t and the dependent variables η and $\overline{\overline{U}} = q/(h+\eta)$ (Equation 11) to the parametric coordinates

$$\sigma^2/16 = x/\mathcal{L}_x + \eta/\mathcal{L}_z, \quad \lambda/2 = t/\mathcal{T} - \overline{\overline{U}}/\mathcal{V} \tag{43}$$

where $\mathcal{L}_x = L$ is a horizontal length scale that characterises the Figure 5 domain, $\mathcal{L}_z = \alpha L$ is the vertical length scale, $\mathcal{T} = \sqrt{L/(g\alpha)}$ is the time scale, and $\mathcal{V} = \sqrt{g\alpha L}$ is the velocity scale. In this transformation, the wetting and drying front is at $\sigma = 0$. The Equation 43 transformation must be single valued for non-breaking waves in the solution domain $\sigma > 0$, which requires that the Jacobian $\partial(x,t)/\partial(\sigma,\lambda)$ of the coordinate transformation never vanishes for $\sigma > 0$.

The analytical solution is written in terms of the potential $\varphi(\sigma,\lambda)$ as

$$\frac{1}{\mathcal{V}}\overline{\overline{U}}(\sigma,\lambda) = -\frac{1}{\sigma}\frac{\partial\varphi}{\partial\sigma}, \quad \frac{1}{\mathcal{L}_z}\eta(\sigma,\lambda) = \frac{1}{4}\frac{\partial\varphi}{\partial\lambda} - \frac{1}{2\sigma^2}\left(\frac{\partial\varphi}{\partial\sigma}\right)^2 \tag{44}$$

Carrier and Greenspan (1958) provide the solution for a standing wave of dimensionless amplitude A and dimensionless frequency ω in the Figure 5 domain, where

$$\varphi(\sigma,\lambda) = AJ_0(\omega\sigma)\cos(\omega\lambda) \tag{45}$$

In this solution, the Jacobian never vanishes for $A \leq 1$.

In application, the dimensional dependent variables $\eta(x,t)$ and $q(x,t)$ are required at specified dimensional independent variables x and t. Noting that the Equations 44 and 45 solution provides the dependent variables as functions of σ and λ, an inverse problem formulation is suggested, in two stages:

(I) Given x and t, solve for σ and λ.

The algorithm is based on Equations 43 and the simultaneous implicit algebraic equations

$$\begin{aligned} f_1(\sigma,\lambda) &= \sigma^2/16 - x/\mathcal{L}_x - \eta/\mathcal{L}_z = 0 \\ f_2(\sigma,\lambda) &= \lambda/2 - t/\mathcal{T} + \overline{\overline{U}}/\mathcal{V} = 0 \end{aligned} \tag{46}$$

in which η and $\overline{\overline{U}}$ follow from Equations 44.

Equations 46 are solved numerically as a routine problem in nonlinear optimisation (using `fminsearch` in matlab).

(II) Given σ and λ, predict η and $\overline{\overline{U}}$ directly from Equations 45 and 44. q is then also available as $\overline{\overline{U}}(h+\eta)$.

The solution for the evolution of the wetting and drying front is a special case of the above algorithm, in which $\sigma = 0$. In stage I, Equation 46a is exact and λ is the only unknown.

Subsequently, Carrier et al. (2003) provided solutions for a transient problem with initial conditions

$$\frac{1}{\mathcal{V}}\overline{\overline{U}}(\sigma,0) = 0, \quad \frac{1}{\mathcal{L}_z}\eta(\sigma,0) = F(\sigma) \tag{47}$$

The solution has the form

$$\varphi(\sigma,\lambda) = 2\int_0^\infty F(b)G(b,\sigma,\lambda)\,db \tag{48}$$

where

$$G(b,\sigma,\lambda) = b\int_0^\infty J_0(\rho\sigma)\sin(\rho\lambda/2)J_0(\rho b)\,d\rho \tag{49}$$

is the Green function. Given a choice of the initial condition $F(\sigma)$, application of Equations 48 and 49 requires extensive numerical integration that must cope with a line singularity in the (σ,λ) domain.

Tinti and Tonini (2005) have observed that the special case initial conditions

$$F(\sigma) = \left(1+\sigma^2\right)^{-3/2}\sum_{k=0}^{3} c_k\left(1+\sigma^2\right)^{-k} \tag{50}$$

have application to nearshore earthquake-induced tsunami runup. The c_k are dimensionless coefficients. Significantly also, the Equation 50 initial conditions lead to solutions to Equation 48 that avoid extensive numerical integration. Tinti and Tonini (2005) provide explicit analytical field solutions for $\overline{\overline{U}}(\sigma,\lambda)/\mathcal{V}$, $\varphi(\sigma,\lambda)$ and $\eta(\sigma,\lambda)/\mathcal{L}_z$ (Tinti and Tonini Equations 3.22 through 3.24). They also provide similarly explicit analytical solutions for the speed of the wetting and drying front $\overline{\overline{U}}(0,\lambda)/\mathcal{V}$, and the water surface elevation at the front $\eta(0,\lambda)/\mathcal{L}_z$ (Tinti and Tonini Equations 3.26 and 3.27). (Note two typographical errors in these explicit solutions. In line 3 of Tinti and Tonini Equation 3.24, $c_2/15$

should be $c_2/5$. In line 2 of Tinti and Tonini Equation 3.27, $c_3/35$ should be $6c_3/35$. These typographical errors have been confirmed by the authors (private communication, May 2008).

In application again, the dimensional dependent variables $\eta(x,t)$ and $q(x,t)$ are required at specified dimensional independent variables x and t. The Equation 46 inverse algorithm remains appropriate.

References

Abramowitz, M. and I. A. Stegun (1964). *Handbook of Mathematical Functions*. Dover, New York.

Ames, W. F. (1969). *Numerical Methods for Partial Differential Equations*. Nelson, London.

Bates, P. D. and J.-M. Hervouet (1998). A new method for moving-boundary hydrodynamic problems in shallow water. *Procs., Royal Society, London (A) 455*, 3107–3128.

Bellotti, G. and M. Brocchini (2001). On the shoreline boundary conditions for Boussinesq-type models. *International Journal for Numerical Methods in Fluids 37*, 479–500.

Bode, L. and R. J. Sobey (1984). Initial transients in long wave computations. *Journal of Hydraulic Engineering, ASCE 110*(10), 1371–1397.

Brocchini, M., I. A. Svendsen, R. S. Prasad, and G. Bellotti (2002). A comparison of two different types of shoreline boundary conditions. *Computer Methods in Applied Mechanics and Engineering 191*, 4475–4496.

Carrier, G. F. and H. P. Greenspan (1958). Water waves of finite amplitude on a sloping beach. *Journal of Fluid Mechanics 4*, 97–109.

Carrier, G. F., W. T.T., and H. Yeh (2003). Tsunami run-up and draw-down on a plane beach. *Journal of Fluid Mechanics 475*, 79–99.

Colebrook, F. C. and C. M. White (1937). Experiments with fluid friction in roughened pipes. *Procs., Royal Society, London (A) 161*, 367–381.

Falconer, R. A. and P. H. Owens (1987). Numerical simulation of flooding and drying in a depth-averaged tidal flow model. *Procs., Institution of Civil Engineers, Part 2, Research and Theory 83*, 161–180.

King, I. P. and L. Roig (1988). Two dimensional finite element models for floodplains and tidal flats. In K. Niki and M. Kawahara (Eds.), *Proceedings of an International Conference on Computational Methods in Flow Analysis, Okayama*, pp. 711–718.

Lamb, H. (1932). *Hydrodynamics* (6 ed.). Cambridge University Press, Cambridge.

Leendertse, J. J. and E. C. Gritton (1971). A water-quality simulation model for well-mixed estuaries and coastal seas: Volume 2, Computational procedures. Report R-708-NYC, Rand Corporation, Santa Monica.

Lynch, D. R. and W. G. Gray (1980). Finite element simulation of flow in deforming regions. *Journal of Computational Physics 36*, 135–153.

Lynett, P. J., T.-R. Wu, and P. L.-F. Liu (2002). Modeling wave runup with depth-integrated equations. *Coastal Engineering 46*, 89–107.

Madsen, P. A., O. R. Sørensen, and H. A. Schäffer (1997). Surf zone dynamics simulated by a Boussinesq type model. Part I. Model description and cross-shore motion of regular waves. *Coastal Engineering 32*, 255–287.

Oey, L.-Y. (2005). A wetting and drying scheme for POM. *Ocean Modelling 9*, 135–150.

Peregrine, D. H. (1967). Long waves on a beach. *Journal of Fluid Mechanics 27*, 815–827.

Prasad, R. S. and I. A. Svendsen (2003). Moving shoreline boundary condition for nearshore models. *Coastal Engineering 49*, 239–261.

Preissmann, A. and J. A. Cunge (1961). Calcul du intumescences sur machines électroniques. In *IX Congress of International Association for Hydraulic Research, Dubrovnik*, pp. 656–664.

Reid, R. O. and B. R. Bodine (1968). Numerical model for storm surges in Galveston Bay. *Journal of Waterways and Harbors Division, ASCE 94*, 33–57.

Sielecki, A. and M. G. Wurtele (1970). The numerical integration of the nonlinear shallow-water equations with sloping boundaries. *Journal of Computational Physics 6*, 219–236.

Sobey, R. J. (2001). Evaluation of numerical models of flood and tide propagation in channels. *Journal of Hydraulic Engineering, ASCE 127*, 805–824.

Sobey, R. J. (2002). Analytical solutions for flood and tide codes. *Coastal Engineering Journal 44*, 25–52. See errata Vol. 44, p. 281.

Stoker, J. J. (1948). The formation of breakers and bores the theory of nonlinear wave propagation in shallow water and open channels. *Communications on Pure and Applied Mathematics 1*, 1–87.

Thacker, W. C. (1977). Irregular grid finite-difference techniques: simulations of oscillations in shallow circular basins. *Journal of Physical Oceanography 7*, 284–292.

Thacker, W. C. (1979). Irregular-grid finite-difference techniques for storm surge calculations for curving coastlines. In J. C. J. Nihoul (Ed.), *Marine Forecasting, Predictability and Modelling in Ocean Hydrodynamics*, pp. 261–283. Elsevier, Amsterdam. Procs., 10th International Liége Colloquium on Ocean Hydrodynamics.

Tinti, S. and R. Tonini (2005). Analytical evolution of tsunamis induced by near-shore earthquakes on a constant slope ocean. *Journal of Fluid Mechanics 535*, 33–64.

Titov, V. V. and C. E. Synolakis (1995). Modelling of breaking and non-breaking long-wave evolution and runup using VTCS-2. *Journal of Waterway, Port, Coastal and Ocean Engineering, ASCE 121*, 308–316.

Wei, G., J. T. Kirby, S. T. Grilli, and R. Subramanya (1995). A fully nonlinear Boussinesq model for surface waves. Part I. Highly nonlinear unsteady waves. *Journal of Fluid Mechanics 294*, 71–92.

Zelt, J. A. (1991). The run-up of nonbreaking and breaking solitary waves. *Coastal Engineering 15*, 205–246.